

no page number (pc78)
EMI_12752 (hn_fanny)
END

Heavy water and ^{15}N labeling with NanoSIMS analysis reveals growth-rate dependent metabolic heterogeneity in chemostats

***Corresponding authors**

Email addresses: skopf@caltech.edu (Sebastian H. Kopf), yunbin@gps.caltech.edu (Yunbin Guan), dkn@caltech.edu (Dianne K. Newman), vorphan@gps.caltech.edu (Victoria J. Orphan)
Heavy water and ^{15}N labeling with NanoSIMS analysis reveals growth-rate dependent metabolic heterogeneity in chemostats

Sebastian H. Kopf^{a,b,c,*}, Shawn E. McGlynn^a, Abigail Green-Saxena^b, Yunbin Guan^{a,c,*}, Dianne K. Newman^{a,b,c,*}, Victoria J. Orphan^{a,*}

^a*Division of Geological and Planetary Sciences, California Institute of Technology, Pasadena, CA, USA*

^b*Division of Biology and Biological Engineering, California Institute of Technology, Pasadena, CA, USA*

^c*Howard Hughes Medical Institute, Pasadena, CA, USA*

Abstract

To measure single cell microbial activity and substrate utilization patterns in environmental systems, we employ a new technique using stable isotope labeling of microbial populations with heavy water (a passive tracer) and ^{15}N ammonium in combination with multi-isotope imaging mass spectrometry. We demonstrate simultaneous NanoSIMS analysis of hydrogen, carbon and nitrogen at high spatial and mass resolution, and report calibration data linking single cell isotopic compositions to the corresponding bulk isotopic equivalents for *Pseudomonas aeruginosa* and *Staphylococcus aureus*. Our results show that heavy water is capable of quantifying in situ single cell microbial activities ranging from generational time scales of minutes to years, with only light isotopic incorporation (~ 0.1 atom % ^2H). Applying this approach to study the rates of fatty acid biosynthesis by single cells of *S. aureus* growing at different rates in chemostat culture (~ 6 hours, 1 day and 2 week generation times), we observe the greatest anabolic activity diversity in the slowest growing populations. By using heavy water to constrain cellular growth activity, we can further infer the relative contributions of ammonium vs. amino acid assimilation to the cellular nitrogen pool. The approach described here can be applied to disentangle individual cell activities even in nutritionally complex environments.

Keywords: stable isotope labeling, NanoSIMS, single cell analysis, multi isotope imaging, metabolic heterogeneity

1. Introduction

This article has been accepted for publication and undergone full peer review but has not been through the copyediting, typesetting, pagination and proofreading process, which may lead to differences between this version and the Version of Record. Please cite this article as doi: 10.1111/1462-2920.12752

A fundamental challenge in environmental microbiology is discerning what microorganisms are doing in diverse habitats. Being able to answer this question quantitatively is an even more elusive goal, yet necessary to predict the effects of microbial activity on environmental processes. Today it is well recognized that microbial communities are diverse; often it is necessary to parse them at the single-cell level in order to understand how heterogeneous populations operate. Though it is possible to gain valuable insights from measuring microbial activities in bulk, without single cell resolution, important features of population biology may be missed. Particularly for individual cells, net anabolic activity for growth and maintenance is a key physiological parameter that reflects use of all available resources, and allows specific activities—such as substrate use—to be properly contextualized. Traditional techniques involving isotopically enriched substrates (e.g. with ^{13}C , ^{15}N , ^{34}S , etc.) have the potential to provide such insight, if their utilization at the single cell level can be measured in combination with that of a universal tracer for general cellular activity.

Multi-isotope secondary ion imaging mass spectrometry (MIMS or NanoSIMS) provides one of the most sensitive and precise analytical methods available to study elemental and isotopic composition at high spatial resolution. This technique has been broadly applied in the field of microbial ecology to study the spatiometabolic activity of diverse microbial communities (Popa et al., 2007; Musat et al., 2008; Orphan et al., 2009; Dekas et al., 2009; Morono et al., 2011; Woebken et al., 2012), soil microbe-mineral co-localization (Herrmann et al., 2006), and symbiotic interactions (Lechene et al., 2007; Foster et al., 2011; Pernice et al., 2012; Thompson et al., 2012) using various ^{15}N labeled isotope tracers. The non-toxic nature of stable isotope labels combined with the high sensitivity and spatial resolution of NanoSIMS has great potential to quantitatively study metabolic processes even within model organisms ranging from microbes to humans (Steinhauser and Lechene 2013). Examples include the application of isotopically labeled ^{15}N -thymidine to trace stem cell division and nuclear metabolism in mice (Steinhauser et al., 2012; Gormanns et al., 2012), ^{13}C -oleic acid to study fatty acid transport in lipid droplets, ^{15}N -leucine to trace protein renewal in kidney cells (Lechene et al., 2006), various ^{15}N labeled amino acids to study protein turnover in hair-cell stereocilia (Zhang et al., 2012), ^{18}O -trehalose penetration into the nucleus of mouse sperm (Lechene et al., 2012), dual ^{13}C and ^{15}N -labeled substrate in microbial activity studies of oral biofilms (Spormann et al., 2008) and the utilization of host-derived substrates by intestinal microbiota Berry et al. (2013). As evidenced by this accelerating body of work, secondary ion mass spectrometry increasingly finds application in disciplines as diverse as geobiology, biogeochemistry, host-microbe interactions and biomedical research (see Wagner (2009), Orphan and House (2009), Steinhauser and Lechene (2013), and Hoppe et al. (2013) for recent reviews). However, many of these disciplines frequently address questions in nutritionally complex environments where substrate specific ^{13}C and ^{15}N based isotopic tracers often capture only a subset of the microbial population.

To overcome the limitations of substrate-specific isotope labels, heavy water ($^2\text{H}_2\text{O}$) was recently shown to be a powerful new tracer in environmental systems due to its advantages as a chemically and nutritionally passive isotopic label, and its potential for combined application with other enriched substrates (Wegener et al., 2012; Kellermann et al., 2012). Heavy water

constitutes a general isotopic tracer because it is utilized by all organisms and provides a unique tool for measuring microbial activity in a diverse range of environments. This is particularly useful in complex systems with slow-growing organisms, numerous carbon and nitrogen sources, and diverse heterotrophic populations, because the introduction of substrate-specific tracers can disturb the concentration and availability of autochthonous nutrients and inflate or bias species-specific measures of activity. In contrast, heavy water is easy to administer both in environmental and medical contexts, does not distort substrate availability to the benefit of some organisms over others, and is stably incorporated during metabolism into fatty acids and other cellular components with stable C-H bonds (and transiently into exchangeable hydrogen bonds).

Additionally, the low natural abundance of ^2H ($^2\text{H} F = 0.0156\text{at}\%$, de Laeter et al., 2003)

enables relatively small isotopic spikes to capture a wide range of microbial activity (hours to months) in a short time span, with higher tracer concentrations enabling detection even of slow environmental populations with generation times of tens to hundreds of years (Hoehler and Jørgensen, 2013). Figure 1 illustrates an example of the theoretically estimated minimal incubation times required to achieve a fatty acid enrichment signal of $\delta^2\text{H} = 5500\text{‰}$ (or

$^2\text{H} F = 0.1\text{at}\%$) with different $^2\text{H}_2\text{O}$ isotopic spikes for a wide range of microbial populations

doubling over the course of an hour to 100 years (see Supplemental Information G for details).

Despite the potential of $^2\text{H}_2\text{O}$ as a tracer for microbial activity in environmental microbiology, its application in multi-tracer NanoSIMS studies has been fundamentally limited by the typical limitations in dynamic mass range encountered in multi-collector SIMS instruments. The CAMECA NanoSIMS 50L, for example, is a widely used multicollector secondary ion mass spectrometer equipped with 7 electron multiplier detectors or faraday cups that provide simultaneous detection of up to 7 masses at a fixed magnetic field strength. Secondary ion mass spectrometry (SIMS) is a destructive technique that uses a the primary ion beam to gradually ablate the analytical target and generate secondary ions. The destructive nature of SIMS can be particularly problematic in the analysis of organic targets that can be sputtered away quickly and are sometimes in short supply. The parallel detection of all ions of interest is thus an important feature of the NanoSIMS 50L, and its large magnet and multi-collection assemblage typically

allow parallel detection of ions with vastly different mass to charge $\left(\frac{m}{z}\right)$ ratios up to $\sim 22:1$

(i.e. the maximum $\frac{m}{z}$ can be 22 times larger than the lowest mass: $\left(\frac{m}{z}\right)_{\text{max}} = 22 \cdot \left(\frac{m}{z}\right)_{\text{lowest}}$).

This allows, for example, routine parallel detection of several of the most important biological

ions with $^{12}\text{C}^-$ at $12.0000 \frac{m}{z}$, $^{14}\text{N}^{12}\text{C}^-$ for measuring N at $26.0031 \frac{m}{z}$, $^{31}\text{P}^-$ at $31.9738 \frac{m}{z}$ and

$^{32}\text{S}^-$ at $31.9721 \frac{m}{z}$ as well as their minor isotopes, $^{13}\text{C}^-$ at $13.0034 \frac{m}{z}$, $^{15}\text{N}^{12}\text{C}^-$ at $27.0001 \frac{m}{z}$

and $^{34}\text{S}^-$ at $33.9679 \frac{m}{z}$. However, due to the low mass of hydrogen, simultaneous measurement of $^1\text{H}^-$ at $1.0078 \frac{m}{z}$ and $^2\text{H}^-$ at $2.0141 \frac{m}{z}$ can only be combined with other ions up to a mass to charge ratio of ~ 22.2 , which allows multi-isotope imaging for H and C in parallel, but not H and N in parallel. This restriction provides a serious impediment to the use of hydrogen labeled isotopic tracers in combination with nitrogen (both an important isotopic tracer and identifying ion for biomass).

One approach to this problem is to use the instrument in magnetic field switching mode, which requires alternating magnetic field strengths for various ions in subsequent frames of the same analysis. However, this approach precludes simultaneous detection of all ions and is significantly more time-consuming because of the need for sequential analyses and frequent cycling of the magnetic field. An alternative approach was employed by Lozano et al. (2013) to measure the $^{12}\text{C}^2\text{H}^-$ vs. $^{12}\text{C}^1\text{H}^-$ ions with a NanoSIMS 50L in experiments with highly ^2H enriched

sphingomeylin lipids ($^2\text{H} F \approx 40 \text{ at\%}$) as tracers, with corrections for isobaric interferences from $^{13}\text{C}^1\text{H}^-$ and $^{12}\text{C}^2\text{H}^-$. Although further improved by modifying the entrance slit (Slodzian et al., 2014), the typical abundance sensitivity achievable on a NanoSIMS 50L is limited in resolving these interferences for environmental tracer experiments with relatively small enrichments close to natural abundance ^2H (Doughty et al., 2014). Another potential method proposed by Slodzian et al. (2014) takes advantage of the deflection plates located in front of the electron multipliers to use electrostatic peak switching for quasi-simultaneous detection of $^{12}\text{C}_2^2\text{H}^-$ and $^{12}\text{C}^{14}\text{N}^-$ (both nominally at 26 Da) without magnetic field switching. However, truly simultaneous detection is not possible and significant isobaric interferences include $^{13}\text{C}_2^-$, $^{12}\text{C}^{13}\text{C}^1\text{H}^-$ and $^{12}\text{C}_2^1\text{H}_2^-$.

In this study, we present an approach for the simultaneous analysis of three biologically relevant isotope systems (hydrogen, carbon and nitrogen) in microbial populations by NanoSIMS. We establish the necessary calibration for the use of $^2\text{H}_2\text{O}$ in single-cell stable isotope tracer work with native and embedded microorganisms (*Staphylococcus aureus* as a model gram-positive, and *Pseudomonas aeruginosa* as a model gram-negative organism) at environmentally relevant levels of ^{13}C , ^{15}N and ^2H enrichment. We demonstrate the combined application of heavy water and ^{15}N ammonium isotope tracers in a study of microbial activity and population heterogeneity of *S. aureus* during growth in continuous culture with generation times ranging from hours to weeks.

2. Results and Discussion

2.1. Simultaneous NanoSIMS analysis of H, C and N isotopes

The combination of heavy water labeling with other commonly used C and N based isotope tracers for NanoSIMS analysis is technically challenging because of the typical limitations in dynamic mass range encountered in multi-collector SIMS instruments ($\sim 22:1$). For this study, we extended the position of detector trolley #1 past its official maximum configuration in our CAMECA NanoSIMS 50L multi-collection assemblage, gaining an effective mass range of 28:1. This configuration precluded the need for any magnetic or electric field switching and allowed

for truly simultaneous detection of the $^1\text{H}^-$, $^2\text{H}^-$, $^{12}\text{C}^-$, $^{13}\text{C}^-$, $^{14}\text{N}^{12}\text{C}^-$ and $^{15}\text{N}^{12}\text{C}^-$ ions with key isobaric interferences well-resolved (MRP for $^{13}\text{C}^-$, $^{14}\text{N}^{12}\text{C}^-$ and $^{15}\text{N}^{12}\text{C}^-$ was 4560, 7530 and 8800, respectively). Because there are no isobaric interferences for $^1\text{H}^-$ and $^2\text{H}^-$ with this analytical setup, small isotopic enrichments of ^2H can be detected and quantified.

Measurement of the ^1H and ^2H ions requires a strong primary beam current because of the low ionization efficiency of hydrogen. In balancing primary beam current, pre-sputtering and analysis time, additional complications arise from the destructive nature of the technique and the faster detection of nitrogen. Pre-sputtering is a process where the sample is bombarded with a higher primary beam current for a short amount of time prior to data collection in order to embed primary ions (Cs^+) in the sample matrix (Hoppe et al., 2013). This greatly improves ionization efficiency, and consequently provides higher secondary ion counts during analysis, but also degrades the sample and changes ionization efficiency differentially depending on the ions. Figure 2 illustrates the change in ion counts per milli-second, both quantitatively (A) and visually (B), for the major isotopes' ions ($^1\text{H}^-$, $^{12}\text{C}^-$, $^{14}\text{N}^{12}\text{C}^-$) as a function of exposing the sample surface (here, a cluster of single whole cells of *P. aeruginosa* on conductive indium tin oxide (ITO) coated glass) to the primary ion beam. The figure shows how Cs^+ beam sputtering increases ionization efficiency up to a maximum, at which point the sample is increasingly degraded, and ion counts drop as the organic material disappears. The major ion maps in Figure 2 illustrate this visually and also highlight the faster detection of nitrogen. This effect requires adapting analytical conditions to optimally capture secondary ions prior to cellular degradation. The corresponding analytical window targeted in this study for all analyses of whole single cells is indicated by the gray band in Figure 2A. Corresponding data on ionization efficiency and sample ablation during analysis of plastic embedded cells appears in Supplemental Information C.

2.2. Single cell calibration

To calibrate the simultaneously acquired measurements of hydrogen, carbon and nitrogen isotopic composition of single cells by NanoSIMS, we compared single cell values of isotopically labeled homogenous cultures of *S. aureus* and *P. aeruginosa* to their independently measured bulk isotopic composition (see Table I.7 for details). This calibration step is particularly important for hydrogen due to the high capacity for H exchange in organic material and the potential mass fractionation effects expected in the SIMS analysis for H isotopes. We elected to calibrate single cell H isotope measurements against their respective bulk membrane fatty acid isotope composition because fatty acids represent a key non-exchangeable cellular H reservoir that can be measured rigorously at low ^2H enrichment. The calibration curve itself reflects all combined isotopic effects associated with sample preparation and analysis (loss, exchange, mass fractionation, combined H pools from all cellular components, etc.) and thus allows an empirical conversion of a single cell NanoSIMS measurement into the representative enrichment of a cell component (the membrane) that is quantitatively interpretable. In light of this being the first application of multi-isotope imaging mass spectrometry with H, C and N simultaneously, it seemed prudent to also calibrate single cell C and N isotope measurements against their respective bulk cell equivalents. Although natural abundance cells of *Escherichia*

coli and spores of *Clostridia* (Davission et al., 2008; Orphan and House, 2009; Dekas and Orphan, 2010) as well as highly ^{15}N enriched ($\sim 50\%$ ^{15}N) cells of *P. fluorescences* (Herrmann et al., 2006) have been used as reference materials for isotopic analysis of whole single cells, to our knowledge, a multi-point calibration curve with enriched isotopic standards has only been reported previously in TOF-SIMS experiments with ^{15}N (Cliff et al., 2002) and does not exist for carbon or nitrogen analysis of free whole cells in NanoSIMS.

Calibration parameters were calculated from $1/\times$ weighted linear regression of the average isotopic composition of all single cells for a given bacterial isotope standard vs. the measured bulk isotopic composition, and are summarized in table 1 for all isotopic standards tested in this study. In calculations of the average isotopic composition of all single cells for a given standard, individual cells were weighted inversely by the predicted Poisson error σ_F in their isotopic measurement (see Supplemental Information B and Fitzsimons et al. (2000); Hayes (2001) for details) to offset the influence of highly imprecise measurements from small ROIs and low ion counts.

Figure 3 shows the calibration curves for single whole cell analyses of fixed *P. aeruginosa* (172 ROIs) and *S. aureus* (222 ROIs), respectively. As expected, the nitrogen isotope compositions of single cells for both organisms mirror the bulk isotopic composition, with near perfect linear correlation and slope close to 1. However, it is important to note that both slopes fall slightly short of 1.0 (0.94 ± 0.06 and 0.91 ± 0.03), suggesting systematic dilution of the cellular isotopic signal from trace nitrogen on ITO coated glass, systematic isotope fractionation in the analytical process (mass fractionation effects in SIMS analysis typically deplete isotope ratios by 1–10% in the heavier isotope, Fitzsimons et al. (2000)), or potential variability of the cellular components due to preparation for SIMS analysis (fixation, dehydration and storage in ethanol). Background analysis of nitrogen ion counts on ITO coated glass indicates that this component, while present, contributes only negligible amounts of nitrogen to the signal (data not shown). Since isotope ratios and fractional abundances of single cells are derived here directly from NanoSIMS ion count measurements without comparison to an authentic reference standard, fractionating effects during ionization and analysis likely contribute to the observed discrepancy. The relative standard deviation (RSD, in % of the measurement) of the single cell measurements of each calibration curve provides an estimate of the measurement uncertainty from the combination of both analytical error as well as biological variation in the standards (Table 1). In the case of nitrogen, the RSD for the *S. aureus* standards (5.7%) suggests higher biological variability in single cell nitrogen than for *P. aeruginosa* (RSD of 1.6%), which is consistent with the wider range of potential nitrogen sources available in the *S. aureus* medium because of the organism's auxotrophy for several amino acids (see Experimental Procedures).

The carbon isotope composition of single *P. aeruginosa* cells (no ^{13}C standards were prepared for *S. aureus*), closely follows the bulk isotopic composition but also falls short, with a slope of 0.73 ± 0.07 . This also suggests a combination of systematic dilution and isotopic fractionation during analysis. Background analysis also indicates a maximal contribution of organic carbon adhered to the ITO coated glass of $\sim 3\%$. However, in the case of carbon, fixed single cells are expected to be slightly offset isotopically from the unfixed bulk population due to the

introduction of near natural abundance carbon in formaldehyde. Musat et al. (2014) recently reported this effect to account for a ~4% dilution of cellular carbon in experiments with *Pseudomonas putida*, which could explain part of the observed offset in the calibration. Even stronger isotope dilution effects have been observed in more elaborate pre-treatment procedures, such as catalyzed reporter deposition fluorescence *in situ* hybridization (CARD-FISH) (Woeckel et al., 2014), and must be taken into consideration for experiments involving this approach. Finally, the hydrogen isotope composition of single cells for both organisms show a robust linear dependence on the bulk membrane fatty acid isotopic composition. The slope is substantially lower than unity (0.67 ± 0.05 for *P. aeruginosa* and 0.59 ± 0.05 for *S. aureus*). This is consistent with the expected effects of hydrogen exchange. While the measured bulk isotopic composition is based on non-exchangeable hydrogen incorporated into membrane fatty acids, the ^2H content of individual cells measured by NanoSIMS is necessarily based on the integrated signal from all cellular hydrogen. Here, we employed a strict multi-step washing protocol for all cultures, with the goal of exchanging all readily exchangeable hydrogen with natural abundance H in the washing solutions. The calibration should allow for conversion of single cell measurements to bulk fatty acid ^2H for cells treated identically. The calibration parameters inferred for *P. aeruginosa* and *S. aureus* suggest, however, that there can be a substantial degree of variability between individual organisms. The observed pattern indicates that *S. aureus* cells contain a higher proportion of hydrogen that exchanges during these washing steps (lower slope) than *P. aeruginosa* (higher slope), which is consistent with the gram-positive (one lipid membrane instead of two), spherical (lower surface to volume ratio) *S. aureus* containing a lower proportion of lipid bound hydrogen than the gram-negative (two lipid membranes), rod-shaped *P. aeruginosa*. In the absence of any isotope fractionation in the detection of hydrogen during NanoSIMS analysis, the observed slopes would indicate that about ~40% of the hydrogen was exchanged with water during the washing steps for *S. aureus*, and ~30% for *P. aeruginosa*. Lastly, single cell isotopic measurements of hydrogen show substantial variability around the mean for both *S. aureus* (RSD of 19%) and *P. aeruginosa* (RSD of 22%), which likely reflects both the statistical uncertainty in the measurements for each single cell from low ion counts of ^2H , as well as random variation in the exact cellular components (highly exchangeable vs. non-exchangeable parts of the cell) sampled by the ion beam during analysis. This aspect of hydrogen isotope measurements of single cells by secondary ion mass spectrometry is a fundamental constraint that limits the ability to resolve small isotopic differences between individual cells, and requires the analysis of many cells (10s to 100s) within a microbial population if isotopically similar communities need to be distinguished. This calibration provides the empirical parameters for inferring the bulk (whole membrane) hydrogen isotopic composition from the analysis of single whole cells of *S. aureus* and *P. aeruginosa*, with the statistical caveats outlined above. While this calibration is likely applicable to other gram-negative and gram-positive cells of similar morphology that are prepared identically for NanoSIMS analysis, extrapolation to other microorganisms has to be interpreted with care. We applied this calibration to study the distribution of single cell growth rates in continuous culture of *S. aureus* as described in section 2.3 below.

We also measured all bacterial isotopic standards in plastic embedded thin section to provide a calibration for NanoSIMS measurements of sectioned samples. Multi-isotope imaging mass spectrometry in thin section vastly expands the range of applicability of this technique to large complex systems, such as highly structured microbial communities (e.g., biofilms and microbial mats, Fike et al. (2008); Woebken et al. (2012); Wilbanks et al. (2014)) or communities associated with plants and animals (e.g. commensal and symbiotic relationships, Lechene et al. (2007); Berry et al. (2013)). The structural support lent by the plastic matrix provides thin-sections with a flat surface that enables high spatial resolution in imaging mass spectrometry due to the lack of strong topological features. It also retards sample destruction by the ion beam. However, plastic resins also contribute significant amounts of carbon and hydrogen that dilute the isotopic signal of enriched cells. It is thus imperative to calibrate and correct any isotopic measurements of single cells embedded in plastic and we present details on this calibration in Supplemental Information C, which should be useful for future NanoSIMS studies requiring embedding prior to analysis.

2.3 Single cell growth diversity in continuous culture

Both environmental and laboratory populations exhibit significant metabolic variation at the single cell level. This heterogeneity is a fundamental aspect of the ecological function and metabolic versatility of microbial communities, yet it is notoriously difficult to capture analytically at the population level. Here, we demonstrate the combined use of hydrogen and nitrogen isotope labeling with secondary ion mass spectrometry to study the activity, heterogeneity and substrate preferences of individual cells in microbial populations growing at different growth rates under controlled conditions in a chemostat. We focused on the common nosocomial pathogen *S. aureus* for these extended growth experiments to minimize the risk of population heterogeneity by physical differentiation through the formation of biofilms, which is of considerable concern with *P. aeruginosa*. *S. aureus* was grown in continuous culture with three different dilution rates (corresponding to generation times of ~6 hours, ~1 day and ~2 weeks), and spiked at steady state simultaneously with both a $^2\text{H}_2\text{O}$ isotope label ($^2\text{H} F_{\text{water}} = 0.248 \text{ at\%}$, 0.246 at\% and 0.275 at\%) as well as a $^{15}\text{NH}_4^+$ label ($^{15}\text{N} F_{\text{NH}_4^+} = 28.0 \text{ at\%}$, 24.9 at\% , 25.0 at\%) as described in the Experimental Procedures. Samples were withdrawn at regular intervals within 1/2 of a generation time for each experimental setup. The hydrogen and nitrogen isotopic composition of individual cells was measured by multi-isotope NanoSIMS and single cell isotopic values were converted to their corresponding bulk population equivalents using the calibrations for *S. aureus* cells presented earlier (overview of single cell data in Figure I.12). The growth activity rate $\mu_{\text{act}} = \mu + \omega_{\text{fa}}$ (representing the combined cellular replication rate μ and fatty acid turnover ω_{fa}) was calculated from the hydrogen isotope measurements for each cell using the equations outlined in Supplemental Information F.

Table 2 summarizes the results and Figure 4A shows the aggregated data for single cell growth activity rates μ_{act} measured from the three continuous culture experiments in comparison with the experimentally set dilution rates for each culture (representing the expected average

replication rate μ). Overall population growth is slightly underestimated by single cell data in the fastest growing culture (6.38 hours), and overestimated at the intermediate (1.24 days) and slowest (13.34 days) generation times. Overestimates at slower growth rates are potentially a consequence of the turnover component (ω_{fa}). Turnover represents the rate of molecular replacement, that is fatty acid degradation and production that is in excess of the biosynthetic rate required purely for cellular replication (μ). Hydrogen from the water isotope tracer is incorporated in both processes and only their combined effect, the overall biosynthetic/growth activity rate (μ_{act}), can be captured at the single cell level. Bacteria are known to modulate the fatty acid composition of their membranes in response to physical and chemical changes in their environment (Zhang and Rock, 2008), but little is known about fatty acid turnover in bacteria growing at steady-state in a chemically stable environment.

The most striking observation, however, is the diversity in cellular activity rates revealed by our data. For comparison, Table 2 includes a simulated data set produced from all single cell measurements of the bacterial standards (Table 1) scaled to the mean of the fastest continuous culture condition (generation time of 6.38 hours). The RSDs of the single cell hydrogen isotope measurements themselves suggest an increase in heterogeneity from the standards, which reflect exponential growth in batch culture, to the chemostat cultures. Typically, well mixed steady-state chemostat cultures are considered to be amongst the most homogenous microbial populations in any experimental system due to the constant medium composition and lack of chemical gradients. While the possibility of spatial differentiation in the chemostat vessels cannot be ruled out, *S. aureus* does not typically form biofilms in this medium, and careful inspection of the vessels after termination of each experiment revealed no cellular attachment. This implies either phenotypic or genotypic differentiation. The observed diversity would not be possible to detect in bulk physiological or isotopic measurements and is revealed here only by inspection at the single cell level. Single cell activity rates appear to be log-normally, rather than normally distributed (illustrated in Figure H.11). Figure 4B shows the histograms and estimated probability density functions for the log-transformed data together with the best fit approximation to log-normal distributions. Differences in the heterogeneity between the simulated standards data set and the chemostat cultures is evaluated statistically by comparing the variances of the growth rate distributions, as listed in Table 2. The observed pattern suggests that the fastest continuous culture condition (generation time of 6.38 hours) is significantly more heterogeneous than the standards (p-value < 0.01) with a less significant increase from the fastest to the next slower (1.24 days) continuous culture (p-value < 0.5). The most significant increase in heterogeneity is seen in the slowest growth condition (p-value < 0.0001). It is noteworthy that the distribution of single cell growth rates at the slowest growth condition hints at a possible bimodal activity pattern with two distinct sub-populations. No clear pattern as to a dependence of growth activity on cell size could be distinguished and it remains an open question what physiological differences precipitate the diversity of activity rates observed for *S. aureus*, and what mechanisms give rise to the diversification. Slight differences in metabolic strategy, for example, could be a potential source of single cell diversity, and could arise from either genetic diversification, or through stochastic gene expression and other purely phenotypic diversification

mechanisms. Previous work on mixed culture chemostats has highlighted microbial assemblages that are functionally stable yet can undergo dramatic phylogenetic variation within the community (Fernández et al., 1999), but genotypic and phenotypic diversification do not require mixed cultures, both have been observed even for single species in homogenous conditions. Maharjan et al. (2007), for example, measured metabolic diversification of initially clonal, single-species populations of *Escherichia coli* grown in glucose limited chemostats after 90 generations, and showed evidence for differentially evolving subpopulations adopting different metabolic strategies for substrate use. Nikolic et al. (2013) on the other hand, studied gene expression of clonal populations of *E. coli* in similar glucose limited chemostats after ~7 generations, and showed evidence for heterogenous expression of metabolic genes. While both mechanisms do likely occur in parallel, the latter (phenotypic diversification) is more likely to play a dominant role at the generational time scales of this study (4–6 generations). Lastly, it is also noteworthy that observations in long term experiments of stationary phase cultures suggest that at any point in time, the population consists of genetically distinct subpopulations that are dynamically increasing and declining over time (Finkel, 2006). While this growth advantage in stationary phase (GASP) phenotype of different subpopulations is mostly reported in the context of batch cultures where chemical conditions are not constant, it is possible that a slow growing chemostat provides an environment that similarly supports increased heterogeneity within the culture.

2.4 Single cell ammonium utilization

In the continuous culture experiments in this study, *S. aureus* has access to both inorganic and organic nitrogen sources in the form of ammonium and various amino acids (details in Experimental Procedures). A single isotopic tracer based on nitrogen (here, $^{15}\text{NH}_4^+$) thus integrates a mixed signal that is affected both by growth, as well as the cells' nitrogen preference. The RSDs of the nitrogen measurements reported at the end of table 2 already suggest a stronger diversification in nitrogen (from 5.7% RSD in the standards to 93% in the slowest growing culture) compared to hydrogen (from 19% to 51%), pointing to pronounced differences in single cell nitrogen preferences. Constraining growth activity independently by using $^2\text{H}_2\text{O}$ as an additional isotope tracer allowed us to deconvolve the ^{15}N signal and infer ammonium utilization on a single cell basis. For each cell, the fraction of nitrogen assimilated from ammonium ($x_{\text{NH}_4^+}$) was estimated from the ^{15}N isotope labeling strength and the

hydrogen-derived growth rate, as detailed in Supplemental Information F. It is important to note that the hydrogen-derived growth activity rates (μ_{act}) include a component of fatty acid turnover (ω_{fa}) that is unlikely to be representative of cellular nitrogen turnover (ω_{N}). To account for this difference, we estimated cellular nitrogen turnover from known rates of protein turnover, considering the vast majority of cellular nitrogen is bound in proteins (Bertilsson et al., 2003), and assuming ammonium incorporation to occur during turnover. Protein turnover in bacteria has been studied most extensively in experiments with *Escherichia coli*, which suggest turnover rates can range from less than 0.25%/hr for rapidly growing batch cultures to 4–5%/hr for non-growing cells (Podolsky, 1953; Koch and Levy, 1955; Ernest Borek, 1958; Mandelstam and

Halvorson, 1960; Mandelstam, 1960; Marr et al., 1963), with similar ranges observed in studies with *Bacillus cereus* (Urbá, 1959) and yeast (Pratt et al., 2002). Pine (1970; 1972) studied protein turnover specifically in continuous culture at varying generation times and found turnover rates to be fairly constant between 2.5%/hr (glucose based growth) and 3%/hr (acetate based growth), independent of growth rate. For this study, we thus used $\omega_N = 2.75\%/hr$ as an estimate for turnover during steady-state growth with a mixture of carbon sources.

Figure 5A shows the aggregated data for single cell ammonium assimilation, indicating the range and median value of nitrogen assimilation from ammonium (vs. amino acids) in each continuous culture experiment. The data indicate that the majority of all cells derive less than ~50% of their nitrogen from ammonium. Such a significant contribution of amino-acid derived nitrogen

$(1 - x_{NH_4^+})$ is consistent with known nutritional requirements of *S. aureus* (Mah et al., 1967;

Lincoln et al., 1995). The precise values of the average nitrogen assimilation depend on the exact protein turnover rate, which is estimated from literature values. Future work that further constrains protein turnover will enable more quantitative assessment of the exact partitioning between N assimilation from inorganic and organic sources both in laboratory and environmental studies.

The most striking observation, however, is the correlation between cell-specific use of ammonium and growth activity illustrated in Figure 5B. Ammonium utilization in the fastest growing culture is negatively correlated (Spearman correlation = -0.63 , p-value $< 10^{-30}$), whereas the intermediate growth condition does not show a statistically significant correlation, and the slowest growing culture is instead positively correlated (Spearman correlation = 0.80 , p-value $< 10^{-30}$). This indicates that cells within a population of *S. aureus* that is growing relatively fast on average (generation time of 6.38 hours) assimilate more nitrogen from *amino acids* when they are growing above the median rate (gray area in panel 1, Figure 5B), whereas cells within a population that is growing relatively slow on average (generation time of 13.34 days) assimilate more nitrogen from *ammonium* when they are growing faster than their peers (gray area in panel 3). These data do not reveal the nature of any potential causal relationship underlying this correlation, but they potentially suggest that utilizing amino acids over ammonium is the optimal strategy for *S. aureus* only in relatively fast growing cultures (generation time of ~6 hours, panel 1) and becomes less advantageous (generation time of ~1.2 days, panel 2), or even disadvantageous at slower growth and nutrient fluxes (generation time of ~13.3 days, panel 3). This overall pattern of a transition from positive to negative correlation of ammonium uptake with cellular growth activity between the slower growth and fast growth conditions, holds up independent of precise protein turnover rates, although we are only just beginning to uncover these single-cell metabolic differences.

2.5 Important constraints on the quantitative use of 2H_2O labels

For practical application, it is important to note that labeling concentrations above the maximum of 20% 2H_2O pictured in Figure 1 are not recommended, because at higher concentrations the heavy isotope starts to significantly affect the solvent properties of water and substitutes for 1H in functional groups, disturbing biological macromolecules. Most organisms including mammals

and insects are usually unaffected by doses of up to ~10%. Although microorganisms can be unaffected by concentrations as high as 20–30% (Kushner et al., 1999), it is important to assess potential inhibitory effects for all targeted microorganisms in an environmental sample when using elevated concentrations of $^2\text{H}_2\text{O}$ above ~10%, because the (partial) inhibition of certain organisms could severely bias activity measurements. We tested the susceptibility of *S. aureus* to varying doses of $^2\text{H}_2\text{O}$ and observed the toxicity threshold observed to fall between 15–20% $^2\text{H}_2\text{O}$ (see Supplemental Information E for details). In the absence of representative laboratory cultures, toxicity thresholds could be assessed directly in environmental samples by monitoring metabolic output (for example, the rate of sulfate reduction or oxygen respiration) in response to increasing $^2\text{H}_2\text{O}$ spikes. However, $^2\text{H}_2\text{O}$ spikes are best used at low doses. In this study, we thus focused specifically on testing $^2\text{H}_2\text{O}$ labeling methods at low $^2\text{H}_2\text{O}$ concentrations (< 0.3 at%) with the goal of environmental application in mind.

For quantitative assessments of ^2H enrichment, it is also important to consider that the anabolic incorporation of hydrogen from water can vary significantly in response to physiological differences (especially autotrophic vs. heterotrophic growth strategies) and substrate preferences (Sessions and Hayes, 2005; Zhang et al., 2009; Valentine, 2009) and should also be assessed carefully for all targeted microorganisms in an environmental sample. For this study, we determined the key physiological parameters for water hydrogen assimilation into fatty acids specifically for *S. aureus* following the approach of Zhang et al. (2009), and report the results in detail in Figure F.10 and Supplemental Information F.

2.6 Conclusion

As we have demonstrated, single-cell multi-isotope labeling with heavy water in combination with ^{13}C and ^{15}N stable isotope tracers can complement traditional spatiometabolic stable isotope studies by providing the context of baseline microbial activity. The use of heavy water as a non-toxic (at concentrations < 10%), fast-diffusing, chemically conservative tracer, combined with the ability to measure relatively small ^2H enrichments at the single cell level

($^{2\text{H}}F \approx 0.1\text{at}\%$), allows microbial activity measurement in a wide range of environmental systems. These range from natural habitats where microorganisms are growing very slowly to *in-vivo* studies where microbial activity is set in response to host-derived growth factors, toxins or other effectors.

Our data reveal heterogeneity in cellular activity at the single cell level even in populations grown under tightly controlled laboratory conditions in continuous culture. Moreover, at this level of resolution, differences in nitrogen assimilation patterns are evident within populations growing at different rates. Future studies will have to determine whether this phenomenon simply reflects random variation between *S. aureus* populations, or perhaps is indicative of a much broader physiological adaptation that is causally linked to turnover rates. Regardless, it is clear that this approach could provide insight into important physiological processes that elude batch analysis. Going forward, the combination of heavy water labeling with specific ^{13}C and ^{15}N labeled substrates, in particular, will enable studies to measure the assimilation of a target substrate at the single-cell level even in organic-rich environments (for example, soils, biofilms,

microbial mats and tissues) while also providing, at the same time, a clear context for activity of all members of the community independent of their use of the target substrate. Similarly, substrate assimilation studies in oligotrophic environmental systems can be understood in the context of overall community activity and can shed light on the direct and indirect impacts of added nutrients.

3 Experimental Procedures

3.1 Bacterial isotope standards

Bacterial hydrogen, carbon and nitrogen isotopic standards for single cell analysis were created by growing a gram-positive organism, *Staphylococcus aureus* (MN8, Kreiswirth et al., 1983), and a gram-negative organism, *Pseudomonas aeruginosa* (PA14, Rahme et al., 1995), with nutrients of different isotopic composition. A phosphate buffered minimal medium at pH 7.2 containing 2.5 g/L NaCl, 13.5 g/L K₂HPO₄, 4.7 g/L KH₂PO₄, 1 g/L K₂SO₄ and 0.1 g/L MgSO₄·7H₂O served as the basis for all experiments. *P. aeruginosa* was grown in this medium with different amounts of ²H₂O (up to 1%, prepared from a 70% stock solution, Cambridge Isotope Laboratories, #DLM-2259-70-1L), 10 mM ammonium chloride (spiked up to 10% ¹⁵N with 98% enriched ¹⁵NH₄Cl, Sigma-Aldrich, #299251) and 10 mM sodium succinate (spiked up to 10% with 99% enriched succinic-1,2-¹³C₂ acid, Sigma-Aldrich, #491977). *S. aureus* was grown in this medium with different amounts of D₂O, 10 mM ammonium chloride (both spiked identically to *P. aeruginosa* cultures) and 10 mM glycerol (¹³C labeling experiments were not the focus of the study and isotopically labeled glycerol was unavailable for the standards at the time). *S. aureus* further exhibits auxotrophy for several amino acids and vitamins (Mah et al., 1967; Lincoln et al., 1995; Aldeen and Hiramatsu 2004) and the medium was amended with 11.5 mg/L proline, 10 mL/L 50x MEM Amino Acid solution (Sigma-Aldrich, #M5550, final amino acid concentrations: 63.2 mg/L arginine, 15.6 mg/L cysteine, 21 mg/L histidine, 26.35 mg/L isoleucine, 26.2 mg/L leucine, 36.3 mg/L lysine, 7.6 mg/L methionine, 16.5 mg/L phenylalanine, 23.8 mg/L threonine, 5.1 mg/L tryptophan, 18.0 mg/L tyrosine, 23.4 mg/L valine) and 100 µg/L thiamine (B1), 100 µg/L nicotinic acid (B3) and 10 µg/L biotin (B7) for all experiments with this organism.

All cells were grown in 50 mL batch cultures aerobically at 37°C, and were inoculated from fresh (exponential) cultures grown on the same medium. Cultures were harvested in mid-exponential phase to ensure as homogenous a population as possible for consistent isotopic composition. Cells were harvested by centrifugation at 4000 rpm for 10 min at 4°C, and washed 5 times by resuspension in 1x phosphate buffered saline (PBS) solution to remove all residual nutrients. Before the last washing step, samples were split into separate aliquots for bulk isotopic analysis and single cell analysis. Aliquots for bulk analysis were pelleted, frozen and stored at -80°C until further processing. Aliquots for single cell analysis were fixed in 1% freshly prepared formaldehyde in PBS (Paraformaldehyde, Electron Microscopy Sciences, #15713) for 2 hours at room temperature, washed once more in 1x PBS and dehydrated in 50% ethanol.

3.2 Continuous culture

Carbon-limited continuous culture experiments at different growth rates were carried out with *S. aureus* growing aerobically at 37°C in a Sartorius Biostat QPlus autoclavable chemostat system

in the same medium used for the *S. aureus* isotope standards (without any isotope enrichment), and amended with 500 µL/L Antifoam 204 (Sigma Aldrich, #A6426). Chemostat vessels with ~550 mL working volume were inoculated from a single colony pre-grown in the same medium and continuous supply of medium was started upon reaching early stationary phase. Overflow from the vessels was continuously removed to maintain a fixed volume, and for each experiment, the exact dilution rate was determined gravimetrically from the total vessel content and medium flow rate. Redox potential, pH and dissolved oxygen were monitored continuously and optical density was measured in aliquots withdrawn aseptically from vessel overflow. Purity of the culture was checked periodically by light and once by epifluorescence microscopy using fluorescent *in situ* hybridization (FISH, Amann et al., 1990) with an *S. aureus*-specific 16S ribosomal RNA probe (5' to 3': GAAGCAAGCTTCTCGTCCG, Kempf et al., 2000). After the monitored physiological parameters reached steady-state (usually within 4–6 generations), chemostat vessels were spiked with 2 mL 70% $^2\text{H}_2\text{O}$ and 150 mg $^{15}\text{NH}_4\text{Cl}$ isotope tracers, and samples for single cell analysis were withdrawn directly from the vessel at regular intervals depending on the dilution rate. Dilution of the tracers from the continuous supply of fresh medium during incubation (to maintain steady-state growth conditions) was accounted for during data evaluation (see Supplemental Information F for details). Samples were washed and fixed the same way as the bacterial isotope standards for single cell analysis. Dehydrated cells were stored in 100% ethanol at 4°C and returned to 50% ethanol prior to analysis. The effective water isotopic composition of the medium in the chemostat vessels after the spike was monitored using a Los Gatos Research DLT-100 liquid water isotope analyzer; the ammonium concentration was monitored using a Dionex DX-500 ion chromatography system with a 5-250 mm IonPac CS16 cation-exchange column and isocratic elution with 38% methanesulfonic acid at a flow rate of 2 mL/min.

3.3 Bulk analysis

All bulk analyses were carried out on homogenized dry biomass from lyophilized cell pellets. For nitrogen and carbon isotope analysis, 300 to 800 µg of cell powder were weighed out into tin capsules in duplicate, and the bulk carbon and nitrogen isotopic composition was determined by EA-ir-MS at the UC Davis Stable Isotope Facility (Davis, CA).

For hydrogen isotope analysis, the average membrane fatty acid hydrogen isotopic composition was used as a measure of bulk ^2H incorporation because, unlike labile N-H or O-H bonds (Katz, 1960; Thomas, 1971), C-H bonds do not exchange hydrogen spontaneously (Sessions et al., 2004). Lyophilized cell pellets were weighed out into ~1 mg aliquots of dry cell mass, transesterified in the presence of acetyl chloride in anhydrous methanol (1:20 v/v) at 100°C for 10 min (Lepage and Roy 1986; Rodríguez-Ruiz et al., 1998), extracted into hexane, and concentrated under a stream of N_2 at room temperature. Fatty acid methyl esters (FAMES) were identified by gas chromatography/mass spectrometry on a Thermo-Scientific Trace DSQ, and analyzed in triplicate for their isotopic composition by GC/pyrolysis/isotope-ratio mass spectrometry on a Thermo-Scientific Delta Plus XP. All data were corrected for the addition of methyl hydrogen during derivatization. Reported bulk hydrogen isotope compositions represent the mass balance weighted average isotopic composition of all major membrane fatty acids.

3.4 Single cell analysis

1 μL aliquots of fixed whole cells suspended in 50% ethanol (both isotopic standards and continuous culture samples) were spotted onto custom-cut, conductive indium tin oxide (ITO) coated glass (TEC15, Pilkington Building Products, Greensboro, NC, USA) and air-dried at room temperature. ITOs were mapped microscopically with a 40x air objective for later orientation and sample identification during secondary ion mass spectrometry.

All samples were analyzed with a CAMECA NanoSIMS 50L (CAMECA, Gennevilliers, France) housed in the Division of Geological and Planetary Sciences at the California Institute of Technology. Whole cells on ITO were analyzed using a $\sim 3.6\text{pA}$ primary Cs^+ beam current with a nominal spot size of $\sim 300\text{ nm}$ and were pre-sputtered with a $\sim 23\text{pA}$ primary Cs^+ beam current (I_{pre}) for 3 to 6 minutes (t), depending on the size of the pre-sputtering area (A), to a cumulative charge density of $\sim 20\text{pC}/\mu\text{m}^2$ ($I_{\text{pre}} \cdot t/A$). Seven masses were collected in parallel ($^1\text{H}^-$, $^2\text{H}^-$, $^{12}\text{C}^-$, $^{13}\text{C}^-$, $^{14}\text{N}^{12}\text{C}^-$, $^{15}\text{N}^{12}\text{C}^-$, $^{28}\text{Si}^-$) using electron multipliers. Individual samples were located using the NanoSIMS CCD camera, and random analytical spots were chosen within a sample area. For all analyses, the beam was rastered over a square region of $10\text{ }\mu\text{m}$ by $10\text{ }\mu\text{m}$ for 15 min per analytical plane/frame. At least two frames were collected per analysis, and all ion images were recorded at 256×256 pixel resolution with a dwell time of 14 ms/pixel. Pre-sputtering was typically carried out on a larger region of at least $15\text{ }\mu\text{m}$ by $15\text{ }\mu\text{m}$ to make sure that the analytical frame was fully within the pre-sputtered area. Analytical parameters including primary beam focus, secondary beam centering and mass resolution for all ions were verified every ~ 30 minutes.

3.5 Quantification

Bulk carbon, nitrogen and hydrogen isotope measurements were recorded in the conventional

δ -notation ($\delta^x = \frac{{}^x R_{\text{sample}}}{{}^x R_{\text{ref}}} - 1$, with $x = {}^{13}\text{C}$, ^{15}N , ^2H) relative to the reference materials VPDB

(${}^{13}\text{C} R_{\text{VPDB}} = \frac{{}^{13}\text{C}}{{}^{12}\text{C}} = 0.0112372$), air (${}^{15}\text{N} R_{\text{Air}} = \frac{{}^{15}\text{N}}{{}^{14}\text{N}} = 0.003676$) and VSMOW

(${}^2\text{H} R_{\text{VSMOW}} = \frac{{}^2\text{H}}{{}^1\text{H}} = 0.00015576$), respectively (de Laeter et al., 2003). To allow consistent

reporting and exact mass balance calculations (see Supplemental Information A for details), all

measurements were converted to fractional abundances ${}^x F$ (${}^{13}\text{C} F = \frac{{}^{13}\text{C}}{{}^{12}\text{C} + {}^{13}\text{C}}$,

${}^{15}\text{N} F = \frac{{}^{15}\text{N}}{{}^{14}\text{N} + {}^{15}\text{N}}$, ${}^2\text{H} F = \frac{{}^2\text{H}}{{}^1\text{H} + {}^2\text{H}}$) using the relation ${}^x F_{\text{sample}} = \frac{{}^x R_{\text{sample}}}{1 + {}^x R_{\text{sample}}} = \frac{\delta^x + 1}{1/{}^x R_{\text{ref}} + \delta^x + 1}$.

Fractional abundances of single cell analyses were calculated directly from raw ion counts and calibrated against bulk measurements (Section 2.2). In this study, the fractional abundance

values of most isotopically enriched standards and samples fall into the percent (10^{-2}) range, and are thus reported in atom percent (at%).

Raw data from all acquired ion images was processed using the open-source MATLAB plugin Look@NanoSIMS (Polerecky et al., 2012). Ion images from multiple frames were corrected for dead time and QSA effect, aligned, and discrete regions of interest (ROIs) were hand-drawn using the $^{14}\text{N}^{12}\text{C}^-$ ion images to identify the cellular outline of individual cells. All ROIs in this study represent individual single cells.

With the primary beam currents and analytical parameters employed in this study, single cells of *S. aureus* and *P. aeruginosa* typically supported the collection of up to three sequential frames before the primary ion beam ablated the cells. Two frames were collected routinely, and individual ROIs were screened for consistency between the isotopic values of two subsequent frames to control for higher quality data not distorted by sample destruction. ROIs with isotopic value F_i in any frame deviating by more than twice the shot noise $2 \cdot \sigma_F$ (see Supplemental Information B for details) and more than 1% from the frames' accumulated average F were discarded.

Single cell total activity growth rates μ_{act} of *S. aureus* were calculated from the single cell hydrogen isotope measurements (converted to bulk equivalents using the calibrations discussed in the text), sampling times, dilution rates and isotopic composition of the medium. μ_{act} represents the combined total biosynthetic activity from cellular replication rates μ and maintenance turnover ω . Ammonium assimilation $x_{\text{NH}_4^+}$ was estimated from single cell nitrogen isotope measurements using hydrogen-based growth rate estimates. All relevant formulae are discussed in detail in Supplemental Information F. For each experimental condition, derived single cell metrics (μ_{act} and $x_{\text{NH}_4^+}$) from all time points were combined for statistical analysis.

Acknowledgements

We thank Nathan Dalleska and the Caltech Environmental Analysis Center for instrumentation that benefited this project, Grayson Chadwick and Kat Dawson for helpful discussions, and members of the Newman and Orphan labs, as well as John Cliff and two anonymous reviewers for constructive criticism that improved the manuscript. This work was supported by grants from the Howard Hughes Medical Institute (HHMI) and the National Institutes of Health (Grant No. 5R01HL117328-03, to D.K.N.), and from the Gordon and Betty Moore Foundation (Grant No. GBMF3780 to V.J.O.). D.K.N. is an HHMI Investigator. S.H.K. is an HHMI International Student Research Fellow.

4 References

- Aldeen, D. A. Hiramatsu, K., May 2004. *Staphylococcus Aureus*. Molecular and Clinical Aspects. Elsevier.
- Amann, R. I., Krumholz, L., Stahl, D. A. Feb. 1990. Fluorescent-oligonucleotide probing of whole cells for determinative, phylogenetic, and environmental studies in microbiology. *Journal of Bacteriology* 172 (2):762–770.
- Berry, D., Stecher, B., Schintlmeister, A., Reichert, J., Brugiroux, S., Wild, B., Wanek, W.,

Richter, A., Rauch, I., Decker, T., Loy, A., Wagner, M., Mar. 2013. Host-compound foraging by intestinal microbiota revealed by single-cell stable isotope probing. *Proceedings of the National Academy of Sciences of the United States of America* 110 (12):4720–4725.

Bertilsson, S., Berglund, O., Karl, D. M., Chisholm, S. W., 2003. Elemental composition of marine *Prochlorococcus* and *Synechococcus*: Implications for the ecological stoichiometry of the sea. *Limnology And Oceanography* 48 (5):1721–1731.

Cliff, J. B., Gaspar, D. J., Bottomley, P. J., Myrold, D. D., Aug. 2002. Exploration of Inorganic C and N Assimilation by Soil Microbes with Time-of-Flight Secondary Ion Mass Spectrometry. *Applied and Environmental Microbiology* 68 (8):4067–4073.

Davission, M. L., Weber, P. K., Pett-Ridge, J., Singer, S., 2008. Development of standards for NanoSIMS analyses of biological materials. Lawrence Livermore National Laboratory.

de Laeter, J. R., Böhlke, J. K., De Bièvre, P., Hidaka, H., Peiser, H. S., Rosman, K. J. R., Taylor, P. D. P., 2003. Atomic weights of the elements. Review 2000 (IUPAC Technical Report). *Pure and applied chemistry* 75 (6), 683–800.

Dekas, A. E., Orphan, V. J., 2011. Identification of diazotrophic microorganisms in marine sediment via fluorescence in situ hybridization coupled to nanoscale secondary ion mass spectrometry (FISH-NanoSIMS). *Methods in enzymology* 486, 281–305.

Dekas, A. E., Poretsky, R. S., Orphan, V. J., Oct. 2009. Deep-sea archaea fix and share nitrogen in methane-consuming microbial consortia. *Science* 326 (5951), 422–426.

Doughty, D. M., Dieterle, M., Sessions, A., Fischer, W. W., Newman, D. K., 2014. Probing the subcellular localization of hopanoid lipids in bacteria using nanoSIMS. *PLoS ONE*.

Ernest Borek, L. P. D. R., May 1958. Protein turnover in microorganisms. *Proceedings of the National Academy of Sciences of the United States of America* 44 (5), 369–374.

Fernández, A., Huang, S., Seston, S., Xing, J., Hickey, R., Criddle, C., Tiedje, J., Aug. 1999. How stable is stable? Function versus community composition. *Applied and Environmental Microbiology* 65 (8), 3697–3704.

Fike, D. A., Gammon, C. L., Ziebis, W., Orphan, V. J., Jul. 2008. Micron-scale mapping of sulfur cycling across the oxycline of a cyanobacterial mat: a paired nanoSIMS and CARD-FISH approach. *Isme Journal* 2 (7), 749–759.

Finkel, S. E., Feb. 2006. Long-term survival during stationary phase: evolution and the GASP phenotype. *Nature Publishing Group* 4 (2), 113–120.

Fitzsimons, I., Harte, B., Clark, R. M., 2000. SIMS stable isotope measurement: counting statistics and analytical precision. *Mineralogical Magazine* 64 (1), 59–59.

Foster, R. A., Kuypers, M. M. M., Vagner, T., Paerl, R. W., Musat, N., Zehr, J. P., Mar. 2011. Nitrogen fixation and transfer in open ocean diatom–cyanobacterial symbioses. *The ISME Journal* 5 (9), 1484–1493.

Gormanns, P., Gormanns, P., Reckow, S., Reckow, S., Poczatek, J. C., Poczatek, J. C., Turck, C. W., Turck, C. W., Lechene, C. P., 2012. Segmentation of multi-isotope imaging mass spectrometry data for semi-automatic detection of regions of interest. *PloS ONE*.

Hayes, J. M., 2001. Fractionation of carbon and hydrogen isotopes in biosynthetic processes. *Geochemistry Of Non-Traditional Stable Isotopes* 43, 225–277.

- Herrmann, A. M., Clode, P. L., Fletcher, I. R., Nunan, N., Stockdale, E. A., O'Donnell, A. G., Murphy, D. V., 2006. A novel method for the study of the biophysical interface in soils using nano-scale secondary ion mass spectrometry. *Rapid Communications in Mass Spectrometry* 21 (1), 29–34.
- Hoehler, T. M., Jørgensen, B. B., 2013. Microbial life under extreme energy limitation. *Nature Reviews Microbiology*.
- Hoppe, P., Cohen, S., Meibom, A., May 2013. NanoSIMS: Technical Aspects and Applications in Cosmochemistry and Biological Geochemistry. *Geostandards and Geoanalytical Research* 37 (2), 111–154.
- Katz, J. J., Dec. 1960. Chemical and Biological Studies with Deuterium. *Am. Scientist* Vol: 48.
- Kellermann, M. Y., Wegener, G., Elvert, M., Yoshinaga, M. Y., Lin, Y.-S., Holler, T., Mollar, X. P., Knittel, K., Hinrichs, K.-U., Nov. 2012. Autotrophy as a predominant mode of carbon fixation in anaerobic methane-oxidizing microbial communities. *Proceedings of the National Academy of Sciences* 109 (47), 19321–19326.
- Kempf, V. A., Trebesius, K., Autenrieth, I. B., Feb. 2000. Fluorescent In situ hybridization allows rapid identification of microorganisms in blood cultures. *Journal of clinical microbiology* 38 (2), 830–838.
- Koch, A. L., Levy, H. R., Dec. 1955. Protein turnover in growing cultures of *Escherichia coli*. *Journal of Biological Chemistry* 217 (2), 947–957.
- Kreiswirth, B. N., Lofdahl, S., Betley, M. J., O'Reilly, M., Schlievert, P. M., Bergdoll, M. S., Novick, R. P., 1983. The Toxic Shock Syndrome Exotoxin Structural Gene Is Not Detectably Transmitted by a Prophage. *Nature* 305 (5936), 709–712.
- Kushner, D. J., Baker, A., Dunstall, T. G., Feb. 1999. Pharmacological uses and perspectives of heavy water and deuterated compounds. *Canadian Journal Of Physiology And Pharmacology* 77 (2), 79–88.
- Lechene, C. P., Hillion, F., McMahon, G., Benson, D., Kleinfeld, A. M., Kampf, J. P., Distel, D., Luyten, Y., Bonventre, J., Hentschel, D., Park, K. M., Ito, S., Schwartz, M., Benichou, G., Slodzian, G., 2006. High-resolution quantitative imaging of mammalian and bacterial cells using stable isotope mass spectrometry. *Journal of Biology* 5 (6), 20.
- Lechene, C. P., Lee, G. Y., Poczatek, J. C., Toner, M., Biggers, J. D., 2012. 3D multi-isotope imaging mass spectrometry reveals penetration of ^{18}O -trehalose in mouse sperm nucleus. *PLoS ONE* 7 (8), e42267.
- Lechene, C. P., Luyten, Y., McMahon, G., Distel, D. L., Sep. 2007. Quantitative imaging of nitrogen fixation by individual bacteria within animal cells. *Science* 317 (5844), 1563–1566.
- Lepage, G., Roy, C. C., Jan. 1986. Direct transesterification of all classes of lipids in a one-step reaction. *Journal of lipid research* 27 (1), 114–120.
- Lincoln, R. A., Leigh, J. A., Jones, N. C., Jul. 1995. The Amino-Acid-Requirements of *Staphylococcus-Aureus* Isolated From Cases of Bovine Mastitis. *Veterinary Microbiology* 45 (2–3), 275–279.
- Lozano, M. M., Liu, Z., Sunnick, E., Janshoff, A., Kumar, K., Boxer, S. G., Apr. 2013. Colocalization of the ganglioside G(M1) and cholesterol detected by secondary ion mass

spectrometry. *Journal of the American Chemical Society* 135 (15), 5620–5630.

Mah, R. A., Fung, D. Y., Morse, S. A., Jul. 1967. Nutritional requirements of *Staphylococcus aureus* S-6. *Applied microbiology* 15 (4), 866–870.

Maharjan, R. P., Seeto, S., FERENCI, T., Feb. 2007. Divergence and Redundancy of Transport and Metabolic Rate-Yield Strategies in a Single *Escherichia coli* Population. *Journal of Bacteriology* 189 (6), 2350–2358.

Mandelstam, J., Sep. 1960. The intracellular turnover of protein and nucleic acids and its role in biochemical differentiation. *Bacteriological Reviews* 24 (3), 289–308.

Mandelstam, J., Halvorson, H., 1960. Turnover of protein and nucleic acid in soluble and ribosome fractions of non-growing *Escherichia coli*. *Biochimica et biophysica acta* 40, 43–49.

Marr, A. G., Nilson, E. H., Clark, D. J., Jan. 1963. The Maintenance Requirement of *Escherichia Coli*. *Annals of the New York Academy of Sciences* 102 (3), 536–548.

Morono, Y., Terada, T., Nishizawa, M., 2011. Carbon and nitrogen assimilation in deep subseafloor microbial cells. In: *Proceedings of the . . .*

Musat, N., Halm, H., Winterholler, B., Hoppe, P., Peduzzi, S., Hillion, F., Horreard, F., Amann, R., Jorgensen, B. B., Kuypers, M. M. M., 2008. A single-cell view on the ecophysiology of anaerobic phototrophic bacteria. *Proceedings of the National Academy of Sciences of the United States of America* 105 (46), 17861–17866.

Musat, N., Stryhanyuk, H., Bombach, P., Adrian, L., Audinot, J.-N., Richnow, H. H., Apr. 2014. The effect of FISH and CARD-FISH on the isotopic composition of ^{13}C - and ^{15}N -labeled *Pseudomonas putida* cells measured by nanoSIMS. *Systematic and Applied Microbiology*, 1–10.

Nikolic, N., Barner, T., Ackermann, M., 2013. Analysis of fluorescent reporters indicates heterogeneity in glucose uptake and utilization in clonal bacterial populations. *BMC Microbiology* 13 (1).

Orphan, V. J., House, C. H., Jun. 2009. Geobiological investigations using secondary ion mass spectrometry: microanalysis of extant and paleo-microbial processes. *Geobiology* 7 (3), 360–372.

Orphan, V. J., Turk, K. A., Green, A. M., House, C. H., Jul. 2009. Patterns of ^{15}N assimilation and growth of methanotrophic ANME-2 archaea and sulfate-reducing bacteria within structured syntrophic consortia revealed by FISH-SIMS. *Environmental Microbiology* 11 (7), 1777–1791.

Pernice, M., Meibom, A., Van Den Heuvel, A., Kopp, C., Domart-Coulon, I., Hoegh-Guldberg, O., Dove, S., Jan. 2012. A single-cell view of ammonium assimilation in coral–dinoflagellate symbiosis. *The ISME Journal* 6 (7), 1314–1324.

Pine, M. J., Jul. 1970. Steady-State Measurement of the Turnover of Amino Acid in the Cellular Proteins of Growing *Escherichia coli*: Existence of Two Kinetically Distinct Reactions. *Journal of Bacteriology* 103 (1), 207–215.

Pine, M. J., 1972. Turnover of intracellular proteins. *Annual Reviews in Microbiology* 26 (1), 103–126.

Podolsky, R. J., 1953. Protein degradation in bacteria. *Archives of Biochemistry and Biophysics* 45 (2), 327–340.

Polerecky, L., Adam, B., Milucka, J., Musat, N., Vagner, T., Kuypers, M. M. M., Jan. 2012.

Look@NanoSIMS – a tool for the analysis of nanoSIMS data in environmental microbiology. *Environmental Microbiology* 14 (4), 1009–1023.

Popa, R., Weber, P. K., Pett-Ridge, J., Finzi, J. A., Fallon, S. J., Hutcheon, I. D., Nealson, K. H., Capone, D. G., Jul. 2007. Carbon and nitrogen fixation and metabolite exchange in and between individual cells of *Anabaena oscillarioides*. *The ISME Journal*, 1–7.

Pratt, J. M., Petty, J., Riba-Garcia, I., Robertson, D., Gaskell, S. J., Oliver, S. G., Beynon, R. J., Aug. 2002. Dynamics of protein turnover, a missing dimension in proteomics. *Molecular & Cellular Proteomics* 1 (8), 579–591.

Rahme, L. G., Stevens, E. J., Wolfort, S. F., Shao, J., Tompkins, R. G., Ausubel, F. M., 1995. Common Virulence Factors for Bacterial Pathogenicity in Plants and Animals. *Science* 268 (5219), 1899–1902.

Rodríguez-Ruiz, J., Belarbi, E. H., Sánchez, J. L. G., Alonso, D. L., 1998. Rapid simultaneous lipid extraction and transesterification for fatty acid analyses. *Biotechnology techniques* 12 (9), 689–691.

Sessions, A., Hayes, J. M., Feb. 2005. Calculation of hydrogen isotopic fractionations in biogeochemical systems. *Geochimica Et Cosmochimica Acta* 69 (3), 593–597.

Sessions, A., Hayes, J. M., Sylva, S., Summons, R., 2004. Isotopic exchange of carbon-bound hydrogen over geologic timescales. *Geochimica Et Cosmochimica Acta* 68 (7), 1545–1559.

Slodzian, G., Wu, T.-D., Bardin, N., Duprat, J., Engrand, C., Guerquin-Kern, J.-L., Apr. 2014. Simultaneous hydrogen and heavier element isotopic ratio images with a scanning submicron ion probe and mass resolved polyatomic ions. *Microscopy and Microanalysis* 20 (2), 577–581.

Spormann, A. M., Behrens, S., Losekann, T., Pett-Ridge, J., Weber, P. K., Ng, W.-O., Stevenson, B. S., Hutcheon, I. D., Relman, D. A., May 2008. Linking Microbial Phylogeny to Metabolic Activity at the Single-Cell Level by Using Enhanced Element Labeling-Catalyzed Reporter Deposition Fluorescence In Situ Hybridization (EL-FISH) and NanoSIMS. *Applied and Environmental Microbiology* 74 (10), 3143–3150.

Steinhauser, M. L., Bailey, A. P., Senyo, S. E., Guillermier, C., Perlstein, T. S., Gould, A. P., Lee, R. T., Lechene, C. P., 2012. Multi-isotope imaging mass spectrometry quantifies stem cell division and metabolism. *Nature* 481 (7382), 516–U131.

Steinhauser, M. L., Lechene, C. P., Aug. 2013. Quantitative imaging of subcellular metabolism with stable isotopes and multi-isotope imaging mass spectrometry. *Seminars in Cell and Developmental Biology* 24 (8–9), 661–667.

Thomas, A. F., 1971. Deuterium Labeling in Organic Chemistry.

Thompson, A. W., Foster, R. A., Krupke, A., Carter, B. J., Musat, N., Vaultot, D., Kuypers, M. M. M., Zehr, J. P., Sep. 2012. Unicellular Cyanobacterium Symbiotic with a Single-Celled Eukaryotic Alga. *Science* 337 (6101), 1546–1550.

Urbá, R. C., Mar. 1959. Protein breakdown in *Bacillus cereus*. *Biochemical Journal* 71 (3), 513–518.

Valentine, D. L., 2009. Isotopic remembrance of metabolism past. *Proceedings of the National Academy of Sciences of the United States of America* 106 (31), 12565–12566.

Wagner, M., 2009. Single-Cell Ecophysiology of Microbes as Revealed by Raman

Microspectroscopy or Secondary Ion Mass Spectrometry Imaging. Annual Review of Microbiology 63, 411–429.

Wegener, G., Bausch, M., Holler, T., Thang, N. M., Prieto Mollar, X., Kellermann, M. Y., Hinrichs, K.-U., Boetius, A., Apr. 2012. Assessing sub-seafloor microbial activity by combined stable isotope probing with deuterated water and ^{13}C -bicarbonate. Environmental Microbiology 14 (6), 1517–1527.

Wilbanks, E. G., Jaekel, U., Salman, V., Humphrey, P. T., Eisen, J. A., Facciotti, M. T., Buckley, D. H., Zinder, S. H., Druschel, G. K., Fike, D. A., Orphan, V. J., Feb. 2014. Microscale sulfur cycling in the phototrophic pink berry consortia of the Sippewissett Salt Marsh. Environmental Microbiology, n/a–n/a.

Woebken, D., Burow, L. C., Behnam, F., Mayali, X., Schintlmeister, A., Fleming, E. D., Prufert-Bebout, L., Singer, S., Hoehler, T. M., Pett-Ridge, J., Spormann, A. M., Wagner, M., Weber, P. K., Bebout, B. M., Aug. 2014. Revisiting N_2 fixation in Guerrero Negro intertidal microbial mats with a functional single-cell approach. The ISME Journal, 1–12.

Woebken, D., Hoehler, T. M., Burow, L. C., Prufert-Bebout, L., Bebout, B. M., Pett-Ridge, J., Spormann, A. M., Weber, P. K., Singer, S. W., Jan. 2012. Identification of a novel cyanobacterial group as active diazotrophs in a coastal microbial mat using NanoSIMS analysis 6 (7), 1427–1439.

Zhang, D.-S., Piazza, V., Perrin, B. J., Rzadzinska, A. K., Poczatek, J. C., Wang, M., Prosser, H. M., Ervasti, J. M., Corey, D. P., Lechene, C. P., Jan. 2012. Multi-isotope imaging mass spectrometry reveals slow protein turnover in hair-cell stereocilia. Nature 481 (7382), 520–524.

Zhang, X., Gillespie, A. L., Sessions, A., Aug. 2009. Large D/H variations in bacterial lipids reflect central metabolic pathways. Proceedings of the National Academy of Sciences of the United States of America 106 (31), 12580–12586.

Zhang, Y. M., Rock, C. O., 2008. Membrane lipid homeostasis in bacteria. Nature Reviews Microbiology 6 (3), 222–233.

Figure 1: **Incubation time requirements.** This figure illustrates the theoretically estimated minimal incubation times required to reach an isotopic enrichment in fatty acid deuterium of

$^2\text{H} F = 0.1\text{at}\%$ or $\delta^2\text{H} = 5500\text{‰}$ (in starting material with natural abundance H isotope composition reflecting the international standard mean ocean water, VSMOW), depending on the strength of the isotopic $^2\text{H}_2\text{O}$ label and the average generation time of a microbial population. Labeling concentrations above 20% $^2\text{H}_2\text{O}$ are not recommended, due to the potential toxic effect on solvent properties and enzyme kinetics (see Section 2.5 for details).

Figure 2: **Ionization efficiency and sample ablation in single cell analysis.** **A:** Ion counts of the major H, C and N ions after various extents of primary ion beam exposure (quantified as cumulative charge density $I_{\text{pre}} \cdot t / A$ from pre-sputtering with primary Cs^+ beam current $I_{\text{pre}} \approx 23$ pA). The gray band indicates the analytical window targeted in this study. **B:** $15\text{ }\mu\text{m} \times 15\text{ }\mu\text{m}$ ion images recorded at the different points (1–4) indicated in A, showing a group of individual *P. aeruginosa* cells. For each ion, the maps are normalized to the highest signal intensity for ease of comparison between ions in the side-by-side visualization. Scale bar is $3\text{ }\mu\text{m}$.

Figure 3: **Calibration curves for single cell vs. bulk isotope analysis.** Isotopic composition of bacterial isotope standards in single cell analysis by NanoSIMS vs. bulk analysis by EA-ir-MS (bulk ^{13}C and ^{15}N) and GC-pyrolysis-ir-MS (bulk fatty acid ^2H). All data are reported in fractional abundances $^x F$ (with $x = ^{13}\text{C}$, ^{15}N and ^2H). Data points represent the mean isotopic composition of all measured single cells. The solid vertical error bars for each data point represent the range that comprises 50% of the single cell data. The dashed vertical whiskers represent the entire range of all single cell measurements. Horizontal error bars represent the total range of measured bulk isotopic composition (smaller than symbol sizes in most cases). Linear regressions are shown with 95% confidence bands.

Figure 4: **Single cell growth rates of *S. aureus* in continuous culture measured by isotope labeling with $^2\text{H}_2\text{O}$.** **A:** Box plots of single cell growth activity rates ($\mu_{act} = \mu + \omega_{fa}$, representing the combined cellular replication rate μ and fatty acid turnover ω_{fa}). Gray bands for each continuous culture experiment represent the range comprising 50% of the single cell data with the black lines indicating the median $\bar{\mu}_{act}$. Whiskers represent the entire range of single cell data. White diamonds represent the experimentally set dilution rate for each culture (equivalent to average population replication rate μ). **B:** Histograms of single cell growth rates normalized to the median $\bar{\mu}_{act}$ for each experiment. All data are plotted on a logarithmic scale. The solid black line shows an estimate of the probability density function that represents the data. The dashed line shows the best fit to a log-normal distribution (i.e. a normal distribution of the log-transformed data). Short vertical black lines show all individual data points.

Figure 5: **Single cell ammonium utilization of *S. aureus* in continuous culture measured by isotope labeling with $^2\text{H}_2\text{O}$ and $^{15}\text{N NH}_4^+$.** **A:** Box plots of single cell nitrogen assimilation from ammonium ($x_{\text{NH}_4^+}$). Gray bands for each continuous culture experiment represent the range comprising 50% of the single cell data with the black lines indicating the median. Whiskers represent the entire range of single cell data. **B:** Correlation plot between cell-specific nitrogen assimilation from ammonium ($x_{\text{NH}_4^+}$) and growth activity rate (μ_{act}), showing how ammonium assimilation changes with growth above/below the median within each population. Dashed vertical lines indicate the median growth activity rate with gray background above the median and white background below the median.

Table 1: Calibration parameters for single cell vs. bulk isotope analysis. Calibration parameters were calculated from 1/x weighted linear regression of the average isotopic composition of all single cells ($^x F_{cells}$) for a given bacterial isotope standard (172 ROIs for *P. aeruginosa* and 222 ROIs for *S. aureus*) vs. the measured bulk isotopic composition ($^x F_{bulk}$). All data are reported in fractional abundances $^x F$ (with $x = ^{13}\text{C}$, ^{15}N and ^2H , see Experimental Procedures for details). Reported errors represent 95% confidence intervals from the regression.

| Organism | Isotope | Calibration range ($^x F_{bulk}$ [at%]) | $^x F_{cells}$ vs. $^x F_{bulk}$ slope | $^x F_{cells}$ vs. $^x F_{bulk}$ intercept $^x F$ [at%] | R^2 | single cell RSD [‡] |
|----------------------|-----------------|--|--|---|-------|------------------------------|
| <i>P. aeruginosa</i> | ^2H | 0.017–0.599 | 0.67 ± 0.05 | 0.0 ± 0.0 | 0.998 | 22% |
| <i>S. aureus</i> | ^2H | 0.013–0.689 | 0.59 ± 0.05 | 0.0 ± 0.0 | 0.997 | 19% |
| <i>P. aeruginosa</i> | ^{13}C | 1.1–10.7 | 0.73 ± 0.07 | 0.1 ± 0.2 | 0.997 | 1.6% |
| <i>P. aeruginosa</i> | ^{15}N | 0.36–10.25 | 0.94 ± 0.06 | -0.0 ± 0.1 | 0.999 | 1.6% |
| <i>S. aureus</i> | ^{15}N | 0.36–4.50 | 0.91 ± 0.03 | 0.0 ± 0.0 | 1.000 | 5.7% |

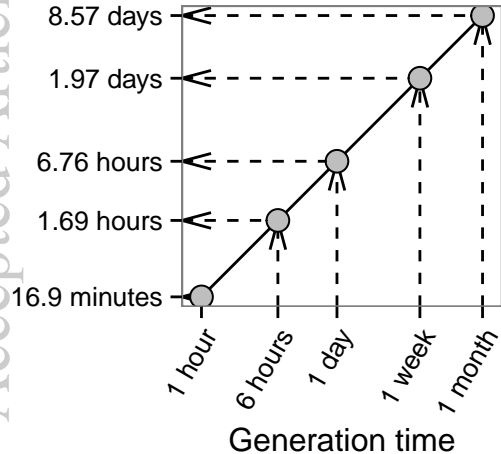
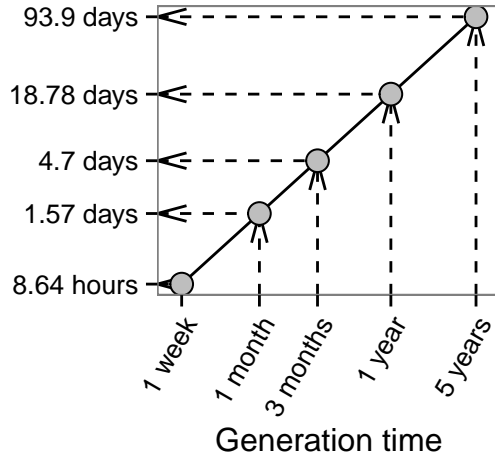
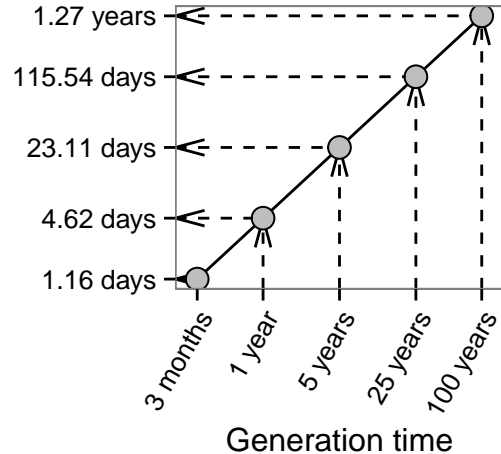
[‡] relative standard deviation (RSD) of all single cell measurements in the calibration (% of the measurement, not at%)

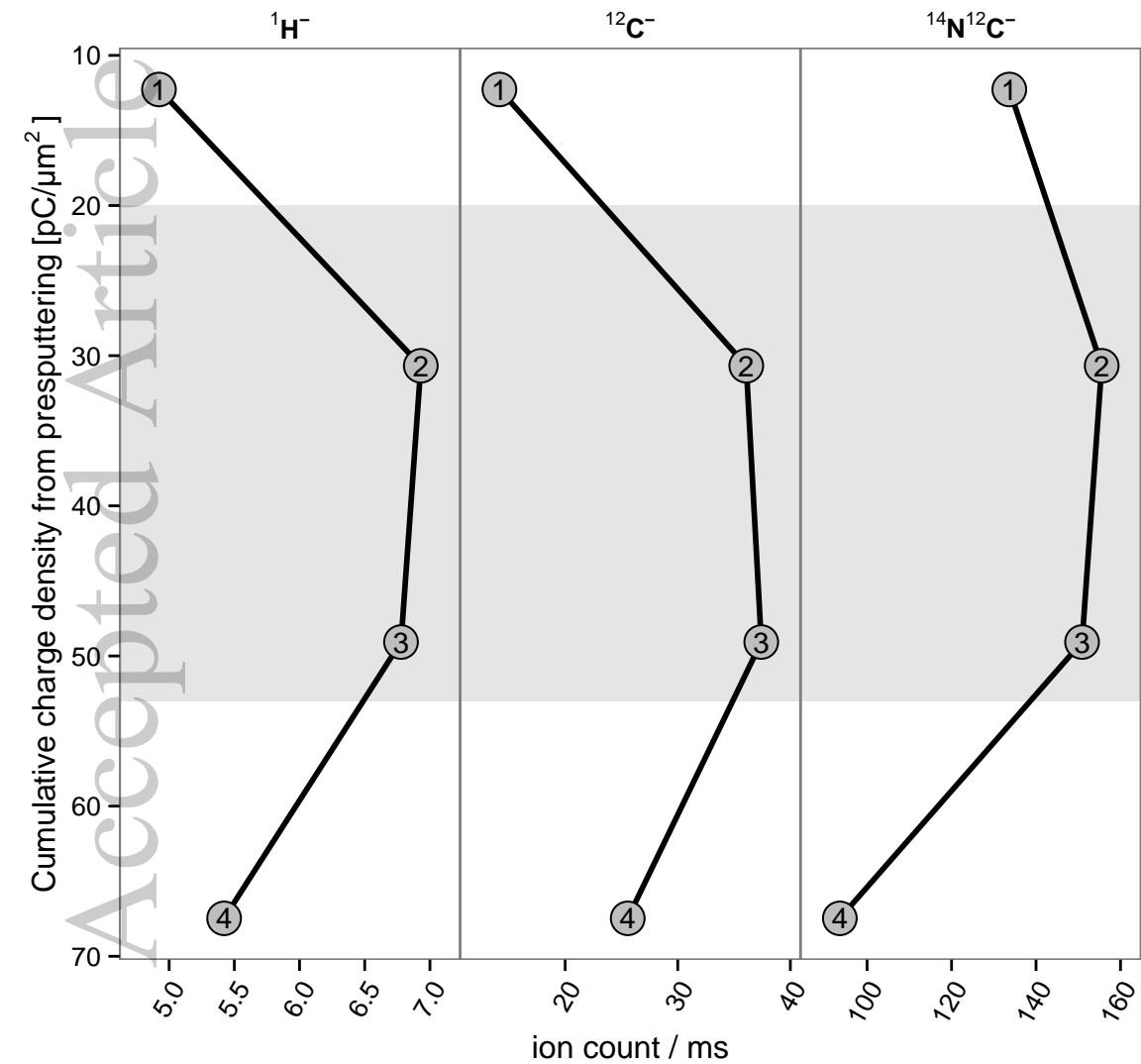
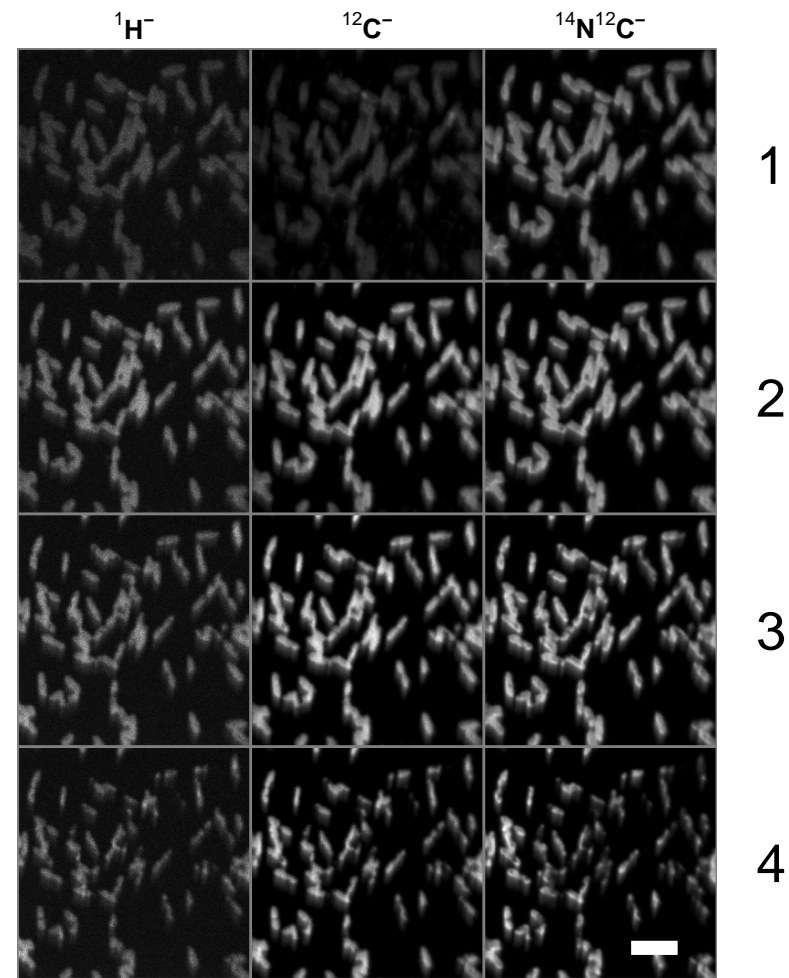
Table 2: Summary of single cell growth rates of *S. aureus* in continuous culture measured by isotope labeling with $^2\text{H}_2\text{O}$. Chemostat parameters are derived from experimental setup. Statistical parameters for each experiment are derived from all individual cells. First line (Standards) is a simulated data set produced from all single cell measurements of the bacterial standards (Table 1) scaled to the mean of the first data set (generation time of 6.38 hours) for statistical comparison and to evaluate propagation of the standards' measurement error (RSD) through the entire growth rate evaluation calculations (see Supplemental Information F for details).

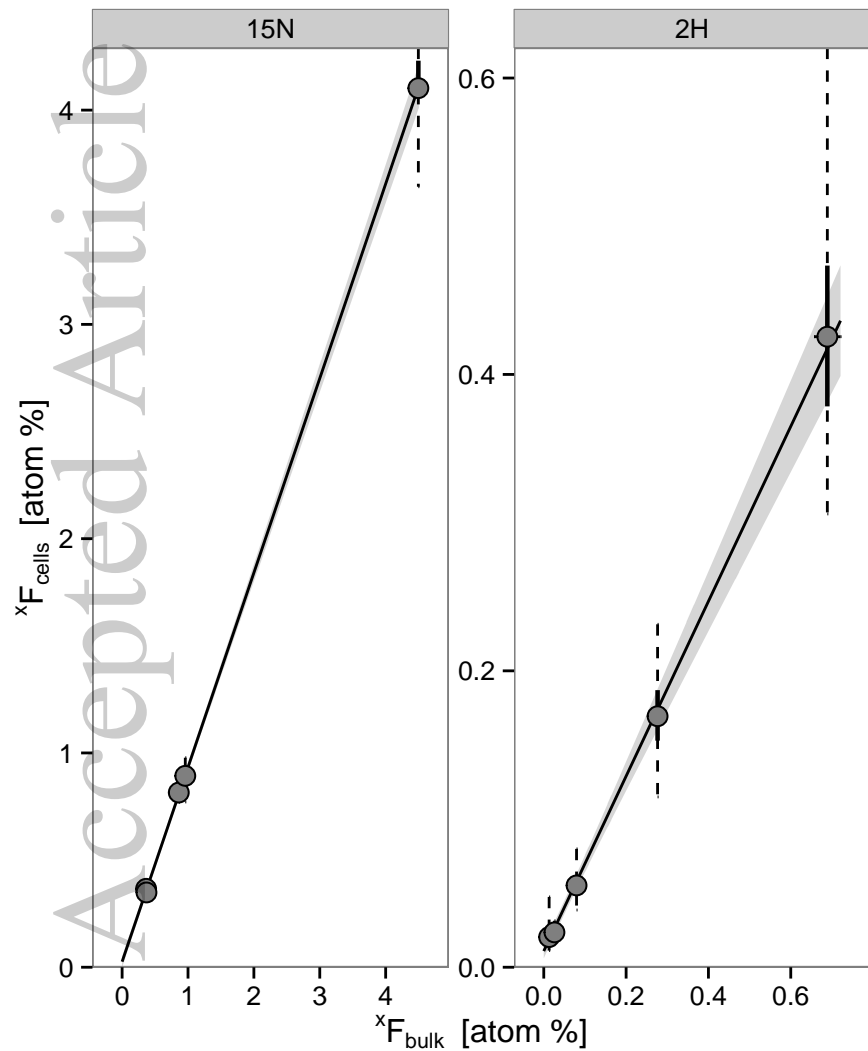
| Dilution rate [hr ⁻¹] | Generation time | Analyzed single cell | Single cell $^2\text{H}_F$ RSD [‡] | Median single cell growth rate $\bar{\mu}_{act}$ [hr ⁻¹] | Single cell growth rate range [50% of data] | Levene's test p-value# | Single cell $^{15}\text{N}_F$ RSD [‡] |
|-----------------------------------|-----------------|----------------------|---|--|--|------------------------|--|
| | | Standards | 19% | 0.102 | $0.65 \cdot \bar{\mu}$ to $1.40 \cdot \bar{\mu}$ | > 0.008 (**) | 5.7% |
| 0.109 | 6.38 hours | 293 | 27% | 0.076 | $0.50 \cdot \bar{\mu}$ to $1.70 \cdot \bar{\mu}$ | > 0.02 (*) | 40% |
| 0.023 | 1.24 days | 296 | 31% | 0.053 | $0.51 \cdot \bar{\mu}$ to $1.80 \cdot \bar{\mu}$ | $> < 0.0001$ (****) | 47% |
| 0.002 | 13.34 days | 188 | 51% | 0.005 | $0.31 \cdot \bar{\mu}$ to $3.50 \cdot \bar{\mu}$ | | 93% |

[‡] relative standard deviation (RSD) of the single cell isotopic measurements (for H and N, respectively)

p-value of the Brown-Forsythe (median-based) Levene-type test statistic for equality of variances between the paired ($>$) growth rate distributions of each consecutive rows, lower p-value indicates higher probability that the variances are *different* (stars indicate standard p-value cutoffs for statistical significance)

1 % ${}^2\text{H}_2\text{O}$ 5 % ${}^2\text{H}_2\text{O}$ 20 % ${}^2\text{H}_2\text{O}$ 

A**B**

S. aureus***P. aeruginosa***